Earth and Planetary Science Letters 285 (2009) 150–162

Contents lists available at ScienceDirect

Earth and Planetary Science Letters

journal homepage: www.elsevier.com/locate/epsl

Gangdese arc detritus within the eastern Himalayan Neogene foreland basin: Implications for the Neogene evolution of the Yalu–Brahmaputra River system

Sara E. Cina [a,*], An Yin [b], Marty Grove [c], Chandra S. Dubey [d], Dericks P. Shukla [d], Oscar M. Lovera [a], Thomas K. Kelty [e], George E. Gehrels [f], David A. Foster [g]

[a] Department of Earth and Space Sciences, University of California, Los Angeles, 3806 Geology, Los Angeles, CA 90095, USA
[b] Department of Earth and Space Sciences and the Institute of Geophysics and Planetary Physics, University of California, Los Angeles, Los Angeles, CA 90095, USA
[c] Department of Geological & Environmental Sciences, Stanford University, Stanford, CA 94305-2115, USA
[d] Department of Geology, University of Delhi, Delhi, 110007, India
[e] Department of Geological Sciences, California State University, Long Beach, CA 90840-3902, USA
[f] Department of Geosciences, University of Arizona, Tucson, AZ 85721, USA
[g] Department of Geological Sciences, University of Florida, Gainesville, Fl 32611, USA

ARTICLE INFO

Article history:
Received 20 August 2008
Received in revised form 20 May 2009
Accepted 5 June 2009
Available online 7 July 2009

Editor: P. DeMenocal

Keywords:
Himalaya
Tibet
evolution of drainage systems
foreland basin
U–Pb detrital zircon dating
Lu–Hf geochemistry
Brahmaputra River

ABSTRACT

In order to assess the spatial and temporal extent of sediment transport from the Gangdese batholith of Tibet to the eastern Himalayan Neogene foreland basin, we performed U–Pb and Lu–Hf analyses on eleven sandstone samples from three locations within the Arunachal and Sikkim Himalaya. We also analyzed detrital zircons from eight modern river sand samples of the Yalu–Brahmaputra River system and its major tributaries in the eastern Himalaya. Results from the river sands are used to contrast the provenance characteristics of the Gangdese arc in southern Tibet with nominally equivalent arc rocks east of the Himalaya in the northernmost Indo-Burma Ranges. Our results indicate that the deposition of Gangdese batholith-derived sediment within the eastern Himalayan foreland: (1) occurred throughout Late Miocene and Pliocene time (~10–3 Ma), (2) was limited to the Arunachal Himalaya, and (3) was sourced north of the Himalaya. This detritus may have been deposited by a transverse Himalayan river, such as the Subansiri River, as suggested by high percentages of the Gangdese-derived zircons within the Neogene samples (15–31%) and S- to SW-oriented paleocurrent directions from two of the Neogene sample localities. At this time, our preferred model to explain the data invokes capture of an originally westward-flowing Yalu River by the Subansiri River at ~10 Ma, followed by capture of the Yalu River by the Siang River at ~3–4 Ma.

1. Introduction

The active Himalayan–Tibetan orogen is an ideal place to investigate the complex interactions among deformation, erosion and climate (e.g., Zeitler et al., 2001). These factors have influenced the evolution of the major Himalayan drainage systems and may have resulted in large-scale reorganizations of the drainage network via mechanisms such as headward erosion, river reversal and river capture (e.g., Burrard and Hayden, 1907; Brookfield, 1998; Clark et al., 2004). Such changes can significantly impact the distribution and intensity of erosion throughout the orogenic system, which in turn can affect the style and location of deformation.

The principal approach for evaluating possible river abandonment, reversal and capture events involves geomorphologic analyses (e.g., Burrard and Hayden, 1907; Brookfield, 1998; Clark et al., 2004). However, when source rocks possess spatially distinct compositional and age properties, provenance analysis emerges as an independent and complimentary tool to record the history of erosion and sediment transport (e.g., Najman, 2006; Najman et al., 2008; Clift et al., 2008). Because the Jurassic–Early Tertiary Gangdese batholith in the Lhasa terrane of southern Tibet is distinct from the largely cratonal rocks of the Himalayan orogen (e.g., Chu et al., 2006; Mo et al., 2007), provenance analysis is an effective approach to determine when and how rivers transported detritus of the Gangdese batholith across the Himalayan Range into the foreland.

The existence of abundant Cretaceous and Early Tertiary Gangdese batholith detrital zircons within Neogene foreland-basin strata in the Arunachal Himalaya (locality A in Fig. 1) was first reported by Cina et al. (2007). To better understand the significance of these results, we have undertaken detrital zircon U–Pb age and Lu–Hf isotopic measurements for samples from modern Himalayan Rivers (localities 1–8 in Fig. 1) and Neogene Himalayan foreland basin strata in the Itanagar and

* Corresponding author. Tel.: +1 310 794 5385; fax: +1 310 825 2779.
E-mail addresses: saracina@ucla.edu (S.E. Cina), yin@ess.ucla.edu (A. Yin), mjgrove@stanford.edu (M. Grove), csdubey@gmail.com (C.S. Dubey), dericks.82@gmail.com (D.P. Shukla), lovera@ucla.edu (O.M. Lovera), tkelty@csulb.edu (T.K. Kelty), ggehrels@geo.arizona.edu (G.E. Gehrels), dafoster@ufl.edu (D.A. Foster).

0012-821X/$ – see front matter © 2009 Elsevier B.V. All rights reserved.
doi:10.1016/j.epsl.2009.06.005

Bhalukpong areas of Arunachal (localities A and B in Fig. 1) and the southern Sikkim Himalaya (locality C in Fig. 1). The results strongly indicate that the Gangdese-age zircon in the eastern Himalayan foreland was deposited by a south-flowing transverse river and was sourced from the Lhasa terrane of southern Tibet, directly north of the range, rather than from a laterally correlative Jurassic–Early Tertiary arc in the Indo-Burma Range to the east. These findings have important implications for the evolution of the Yalu–Brahmaputra River system and suggest possible roles for Himalayan transverse rivers in disrupting first-order longitudinal rivers as a result of tectonic or climatic events.

2. Background

2.1. The Yalu–Brahmaputra River system

Burrard and Hayden (1907) divide the Himalayan drainages into the longitudinal and transverse rivers: the former flow parallel to the orogen and cut across the Himalaya at its eastern and western syntaxes (i.e., the Indus and Yalu–Brahmaputra Rivers), while the latter flow southward perpendicular to the range (e.g., the Teesta, Manas, and Subansiri Rivers) (Fig. 1). Among these, the origin and evolution of the Yalu–Brahmaputra River have been most debated.

Exactly how far back in time the Yalu–Brahmaputra River system has connected the Lhasa terrane of Tibet with the Himalayan foreland basin is uncertain (Fig. 1). Although Burg et al. (1998) have proposed that the Yalu–Brahmaputra River system is long-lived and antecedent to the Himalaya, most researchers consider the establishment of the current drainage configuration in the Eastern Himalaya to be a Late Neogene event. For example, Seeber and Gornitz (1983) suggested that the Yalu River once linked up with the Lohit River while Brookfield (1998) alternatively postulated that the Yalu connected with the Irrawaddy via the Parlung River until ca. 10 Ma, before the Yalu and Brahmaputra Rivers became linked. Clark et al. (2004) and Zeitler et al. (2001) also favored Brookfield's (1998) scenario but suggested more recent capture of the Yalu River by the Brahmaputra at ca. 3–4 Ma. Although the Yalu may never have drained eastward into the South China Sea via the Red River as suggested by Clark et al. (2004), it still may have connected with the south-flowing Irrawaddy or Salween Rivers prior to establishing its current course (Clift et al., 2008; Liang et al., 2008).

Uplift of the eastern syntaxis has been directly related to focused exhumation driven by the incision of Yalu–Brahmaputra River (the tectonic aneurysm hypothesis — see Zeitler et al., 2001; Koons et al., 2002; cf., Ding et al., 2001). The correlation of current topography and $^{40}Ar/^{39}Ar$ biotite and (U–Th)/He zircon cooling ages at the eastern syntaxis, and the dominance of detrital zircons derived from the syntaxis immediately downstream, support rapid and focused erosion there in the latest Pliocene and Quaternary (Finnegan et al., 2008; Stewart et al., 2008).

It has also been proposed that south-flowing Himalayan transverse rivers with catchments extending north of the range crest are antecedent (Fig. 1; Medlicott, 1868; Burrard and Hayden, 1907; Hayden, 1907; Heron, 1922; Wager, 1937), and one or more of these rivers may have carried south Tibetan detritus across the Himalaya into the foreland basin at the start of the Indo-Asian collision (Ding et al., 2005; Yin, 2006). If true, the progressive uplift of the Himalaya ultimately defeated these south-flowing rivers and led to the establishment of the markedly longitudinal, modern Yalu–Brahmaputra and Indus drainage systems.

2.2. Contrasting age and isotopic properties of the Lhasa terrane and Himalayan orogen

Zircon crystallization ages and Hf isotopic compositions differ significantly between the Lhasa terrane and the Himalayan orogen. The former is composed largely of Jurassic to Early Tertiary arc rocks whereas the Himalayan orogen consists primarily of variably metamorphosed Proterozoic–Eocene strata with minor Miocene leucogranites.

The Lhasa terrane consists of 530 Ma and 850 Ma orthogneiss overlain by Ordovician–Cenozoic sedimentary and volcanic sequences (Yin and Harrison, 2000; Guynn et al., 2006). It is extensively intruded in the south by Jurassic–Early Tertiary (200–40 Ma) granitoids of the Gangdese Batholith (e.g., Honegger et al., 1982; Allègre et al., 1984; Schärer et al., 1984; Xu et al., 1985; Debon et al., 1986; Harris et al., 1988; Quidelleur et al., 1997; Harrison et al., 2000; Dong et al., 2005; Mo et al., 2007). The batholith is overlain by the 65–40 Ma Linzizong volcanic sequence (e.g., Coulon et al., 1986; Murphy et al., 1997). The Lhasa terrane also exposes minor post-collisional volcanic rocks and dikes with ages ranging from 30 Ma to 8 Ma (Coulon et al., 1986; Miller et al., 1999; Williams et al., 2001; Kapp et al., 2005; Chung et al., 2005; Mo et al., 2006, 2007).

The Himalayan orogen consists of lithologic units juxtaposed by major north-dipping faults: the Tethyan Himalayan Sequence (THS), the Greater Himalayan Crystalline Complex (GHC), and the Lesser Himalayan Sequence (LHS) (Fig. 1; LeFort, 1996; Hodges, 2000; Yin, 2006). The Upper Proterozoic to Eocene THS was deposited in the northern margin of the Indian continent and is dominated by marine carbonate and clastic sediment (LeFort, 1996). It contains volcanic horizons deposited in the Early Permian (Garzanti et al., 1999), Early–Middle Triassic (250–220 Ma) and Early Cretaceous (~133–132 Ma) (LeFort and Raï, 1999; Zhu et al., 2005b, 2006). The GHC hosts Upper Proterozoic and Paleozoic strata that have been metamorphosed to amphibolite facies as well as 500 Ma and locally 830–870 Ma orthogneiss units in the western and eastern Himalaya (Singh et al., 2002; Yin et al., 2006). The LHS consists of low-grade Precambrian strata locally overlain by Early Paleozoic sequences correlative to those in the THS (Myrow et al., 2003; Yin, 2006).

2.3. Himalayan foreland basin strata

Strata in the Himalayan foreland basin preserve a partial record of the Indo-Asian collision and development of the Himalayan orogen (Najman, 2006). Plate reconstructions and geologic data indicate that collision between the Indian and Asian continents began at 60 ± 10 Ma (see Yin and Harrison, 2000; cf. Zhu et al., 2005a). The effect of Indo-Asian collision in the Himalayan foreland basin was marked by shifts in isotopic composition and detrital zircon provenance (DeCelles et al., 1998; Najman et al., 2000; DeCelles et al., 2004). Although many researchers consider the Upper Eocene and Oligocene strata to be absent in the Himalaya foreland basin (e.g., DeCelles et al., 1998; Najman, 2006), new paleontologic data suggest that they may be locally present (Acharyya, 2007).

Our study of the Himalayan foreland basin strata is focused on sediments in the Sikkim and Arunachal Himalaya. In Sikkim (88–89°E, Fig. 1), the Cenozoic stratigraphy consists of the Lower to Middle Miocene Chunabati Formation and Upper Miocene to Pliocene Middle and Upper Siwalik Group (Fig. 2) (Acharyya and Sastry, 1976; Acharyya, 1999). In Arunachal (92–94°E, Fig. 1), the Upper Miocene Dafla and Subansiri Formations and the Pliocene Kimin Formation are present (Fig. 2) (Kumar, 1997).

3. U–PB dating and LU–HF isotopic analysis of detrital zircon

3.1. Geologic settings of the samples

We collected Neogene samples from two locations (Itanagar and Bhalukpong, localities A and B in Fig. 1) in the Arunachal Himalaya (92–97°E) and a third location in the Sikkim Himalaya (88–89°E) (locality C in Fig. 1). The Itanagar area exposes the Upper Miocene Dafla Formation in the hanging wall and the Miocene Subansiri and Pliocene Kimin Formation in the footwall of the Tipi Thrust (Figs. 1 and 2) (Kumar, 1997). The Dafla Formation is >1200 m thick and has thickly bedded (5–8 m) coarse-grained sandstone interbedded with thinly bedded claystone and siltstone. The lower part of the Subansiri Formation is lithologically similar

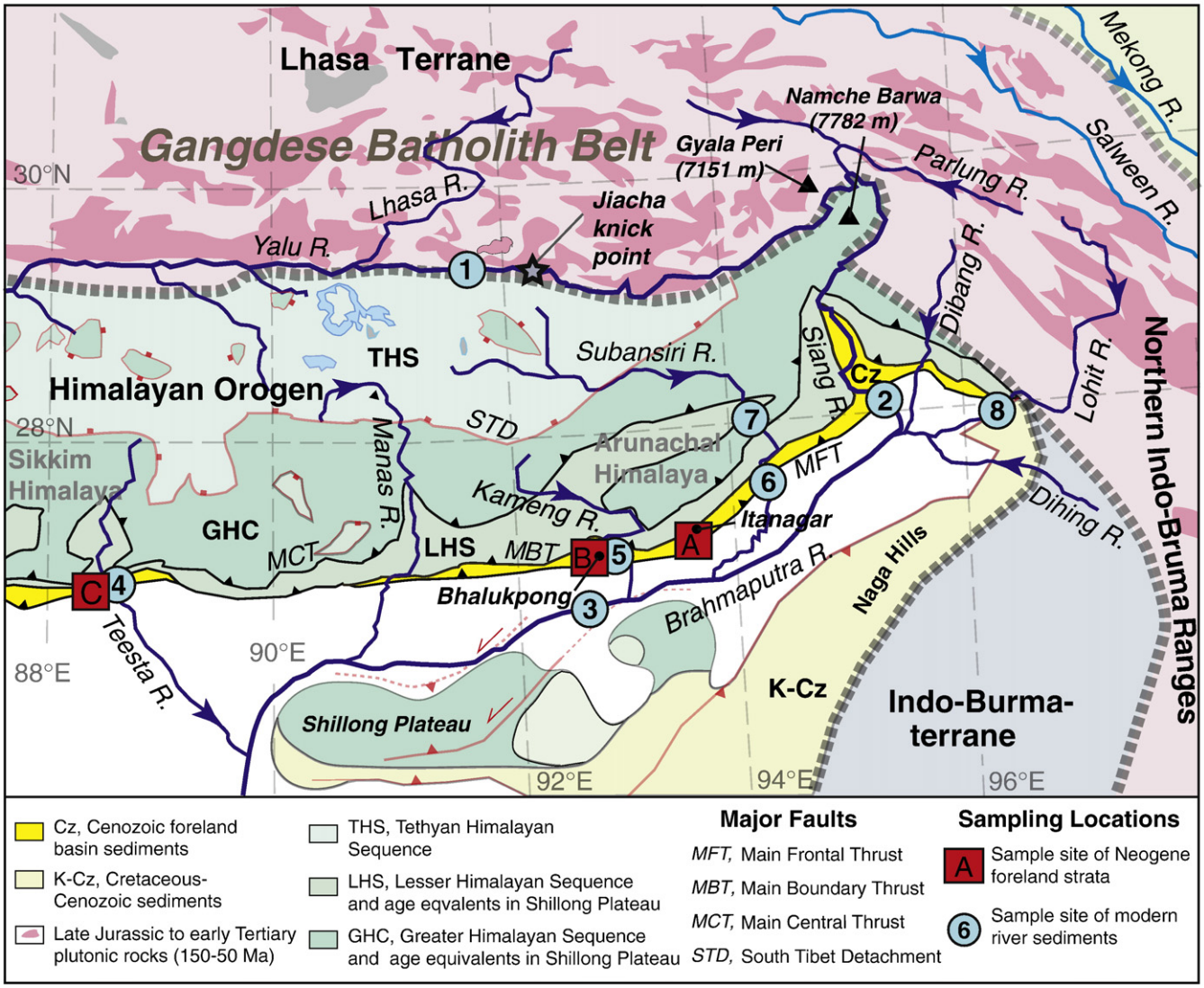

Fig. 1. Regional tectonic map showing simplified geology, locations of major rivers, and sample localities. Sites 1–8 are modern river sands. Locations A, B, and C show Neogene foreland basin localities. Samples AY09-11-03-(1A/B), AY02-07-06-(8), AY02-07-06-(13) are in locality A, samples AY02-12-06-(9), AY02-12-06-(5), AY02-11-06-(6) are in locality B, and samples AY02-20-06-(2), AY02-20-06-(3), AY02-19-06-(10) are in locality C (see Table 1).

to the Dafla Formation, but has sandstone interlayered with conglomerate in its upper section. In the Kimin Formation, conglomerate predominates with minor interlayered siltstone and sandstone. Pebble imbrications in the Kimin Formation and trough cross-bedding laminations in the middle and upper parts of the Subansiri Formation indicate south to southwest paleocurrent directions (Fig. 2). Four sandstone detrital zircon samples were collected near Itanagar. Samples AY09-11-03-(1) and AY09-11-03-(1)B were from the basal Dafla Formation, sample AY02-07-06-(13) from the lowermost Subansiri Formation, and sample AY02-07-06-(8) from the upper Kimin Formation.

The Dafla, Subansiri and Kimin Formations are also exposed in the Bhalukpong area ~130 km west of the Itanagar area (locality B in Fig. 1) (Kumar, 1997). Here cross-bedding lamination is well developed in the Subansiri Formation and indicates S10°W to S30°W paleocurrent directions. Three Neogene samples were collected from the Dafla (sample AY02-12-06-(9)) and Subansiri Formations (samples AY02-11-06-(6) and AY02-12-06-(5)) (Fig. 2).

The Sikkim Himalaya (locality C in Fig. 1) exposes two Tertiary units: the Lower to Middle Miocene Chunabati Formation and Upper Miocene to Pliocene Middle and Upper Siwalik Group (Acharyya, 1999). The Chunabati Formation consists of claystone, siltstone, sandstone and locally limestone, whereas the Siwalik strata have coarse-grained sandstone and conglomerate. Three detrital-zircon samples were collected from the Sikkim Himalaya (Fig. 2). Sample AY02-19-06-(10) was from thickly bedded (3–5 m) coarse-grained sandstone in the uppermost Chunabati Formation. Sample AY02-20-06-(2) was from a sandstone bed in a dominantly conglomerate sequence high in the Upper Siwalik Group. Sample AY02-19-06-(3), also from a sandstone layer stratigraphically underlies AY02-19-06-(2).

Modern sand samples were collected from three types of rivers with distinctive provenances: (1) the Yalu–Brahmaputra system including the Yalu, Siang, and Brahmaputra segments (locations 1–3 on Fig. 1) draining both the Lhasa terrane and Himalayan orogen, (2) transverse rivers (Kameng, Subansiri, and Teesta Rivers, locations 4–7 on Fig. 1) that lie west of the eastern Himalayan syntaxis and presently drain only the Himalayan orogen, and (3) a transverse river in the Indo-Burma Range located east of the eastern Himalayan syntaxis that drains both the Himalayan orogen and the Lhasa terrane (Lohit River, location 8 on Fig. 1). The locations of the seven river sand samples are shown in Fig. 1 and listed in Table 1.

3.2. Methods

We employed standard crushing, sizing, density, and magnetic methods to extract detrital zircons from sandstone and river sand

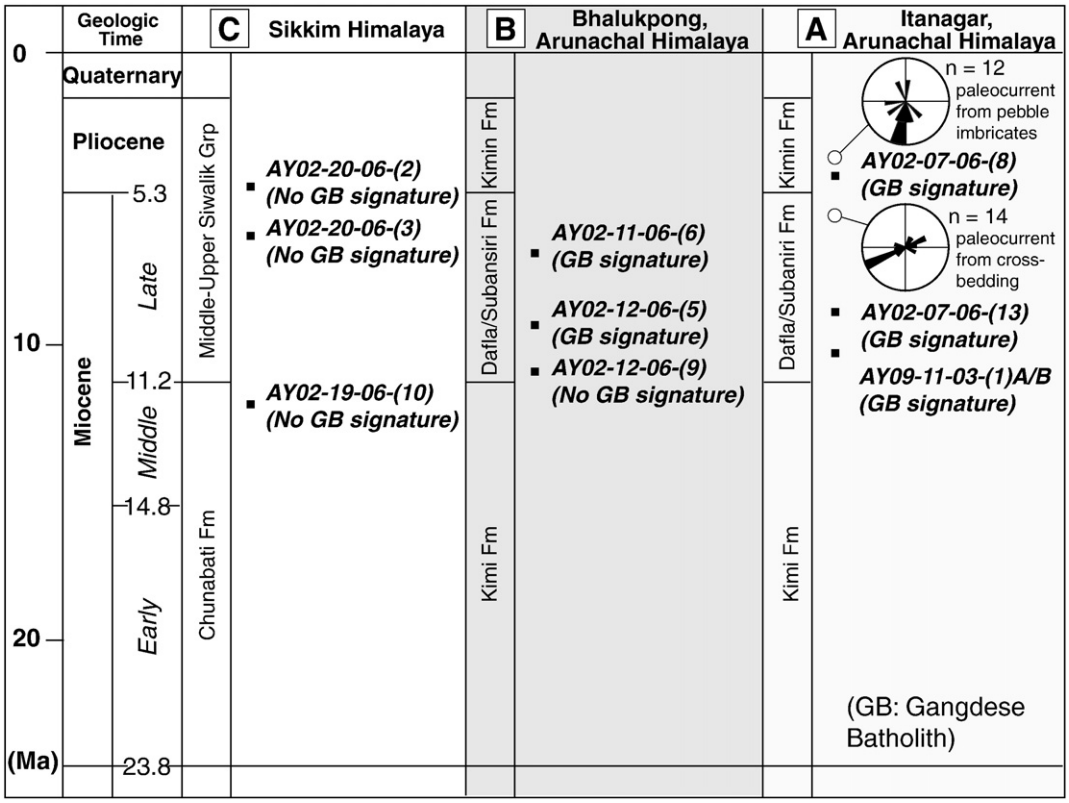

Fig. 2. Nomenclature of Miocene to Quaternary chronostratigraphy in Sikkim (Acharyya and Sastry, 1979) and Arunachal Himalaya (Kumar, 1997; Itanagar and Bhalukpong areas). Approximate stratigraphic positions of Neogene samples are shown based upon geologic map location and field measurements. Approximate stratigraphic positions of measured paleocurrent data in the Itanagar locality are shown.

samples. Laser ablation, multicollector, inductively coupled mass spectrometry (LA-MC-ICP-MS) methods were applied to measure U–Pb age distributions at The University of Arizona's LaserChron facility (Gehrels et al., 2006). Based upon these results, a subset of the analyzed grains was further selected for additional Lu–Hf measurements, also using LA-MC-ICP-MS methods at the University of Florida (Mueller et al., 2008). Because we were interested in differentiating zircons potentially derived from different segments of the Gangdese batholith (Fig. 1), we only carried out Lu–Hf measurements with zircons younger than 200 Ma. Complete U–Pb and Lu–Hf data tables and additional analytical details are presented in the data repository document that accompanies this paper. U–Pb age results are displayed in Figs. 3 and 4 while Lu–Hf data are shown in Fig. 5.

3.3. Detrital zircon U–Pb age distributions from modern river sands

3.3.1. Yalu–Brahmaputra system

3.3.1.1. Yalu River. Sample AY06-28-06-1 (location 1 in Fig. 1) was collected in southeast Tibet near Zedong. The river sand is dominated

Table 1
Sample locations.

Sample name	Description	Latitude (°N)	Longitude (°E)	Location details
AY09-11-03-(1A)	Dafla Fm. sandstone	27.1038	93.6247	Itanagar area, loc. A in Fig. 1
AY09-11-03-(1B)	Dafla Fm. sandstone	27.1038	93.6247	Itanagar area, loc. A in Fig. 1
AY02-07-06-(8)	Kimin Fm. sandstone	26.9816	93.6073	Itanagar area, loc. A in Fig. 1
AY02-07-06-(13)	Subansiri Fm. sandstone	27.0163	93.6188	Itanagar area, loc. A in Fig. 1
AY02-12-06-(9)	Dafla Fm. sandstone	27.0624	92.5936	Bhalukpong area, loc. B in Fig. 1
AY02-12-06-(5)	Subansiri Fm. sandstone	27.0047	92.6417	Bhalukpong area, loc. B in Fig. 1
AY02-11-06-(6)	Subansiri Fm. sandstone	27.0353	93.6254	Bhalukpong area, loc. B in Fig. 1
AY02-20-06-(2)	U. Siwalik Grp. sandstone	26.9154	88.4639	Teesta River area, loc. C in Fig. 1
AY02-20-06-(3)	L. Siwalik Grp. sandstone	26.9072	88.4713	Teesta River area, loc. C in Fig. 1
AY02-19-06-(10)	Chubabati Fm. sandstone	26.8354	88.3422	Teesta River area, loc. C in Fig. 1
AY06-28-06-(1)	Yalu River modern sand	29.3228	91.0921	Loc. 1 in Fig. 1
SC03-26-08-(6)	Siang River modern sand	28.0768	95.3356	Loc. 2 in Fig. 1
AY02-21-06-(2)	Brahmaputra River modern sand	26.6108	92.8536	Loc. 3 in Fig. 1
SK08-A	Teesta River modern sand	26.8816	88.4765	Loc. 4 in Fig. 1
AY02-23-06-(1)	Kameng River modern sand	27.0149	92.6470	Loc. 5 in Fig. 1
SC03-26-08-(4)	Subansiri River modern sand	27.4517	94.2526	Loc. 6 in Fig. 1
AY01-05-09-(1A)	Subansiri River modern sand	28.0054	94.2028	Loc. 7 in Fig. 1
SC03-26-08-(5)	Lohit River modern sand	27.8781	96.3600	Loc. 8 in Fig. 1

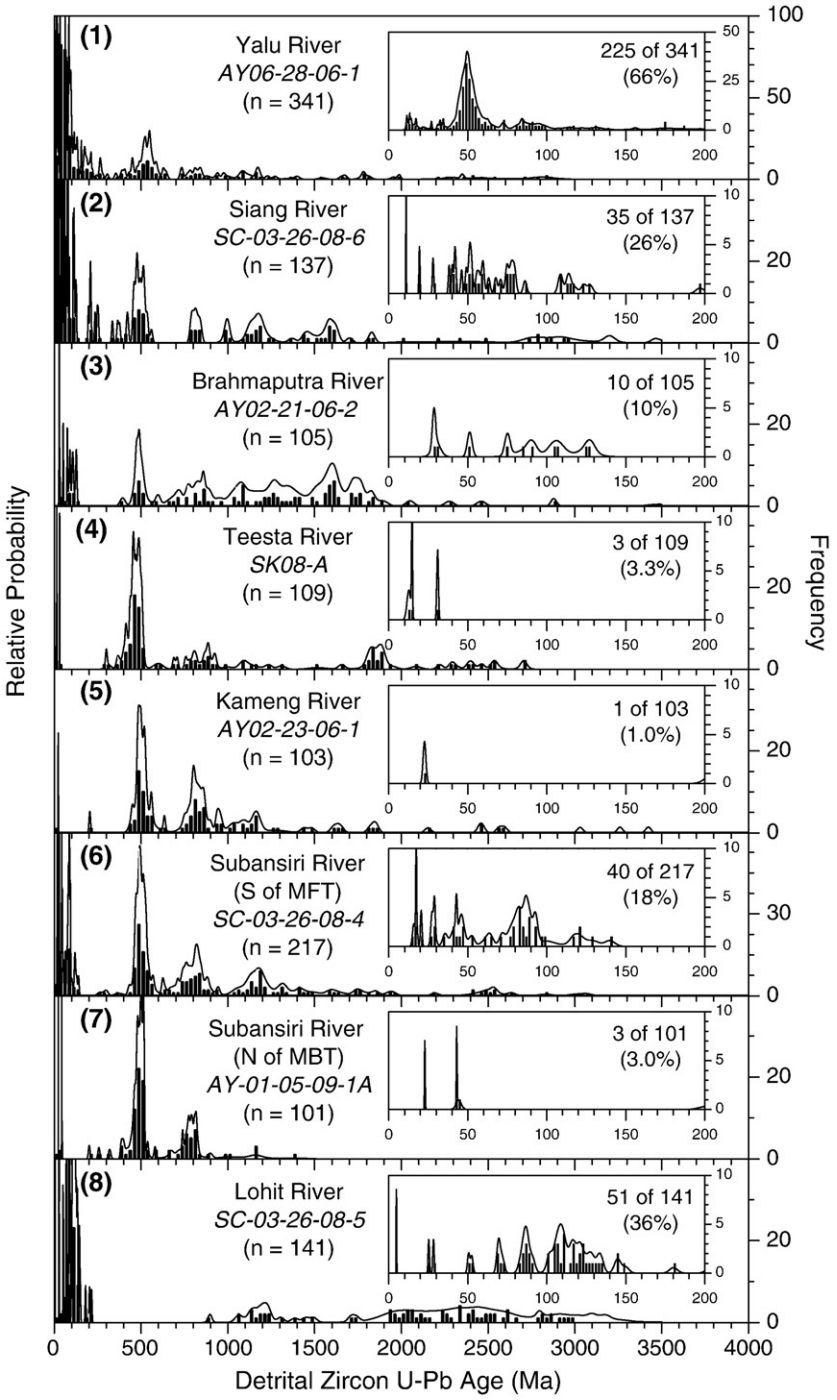

Fig. 3. Histograms and relative probability plots of detrital zircon U–Pb age distributions of modern river sand from locations 1–8 on Fig. 1 and Table 1. Insets show detail in 0–200 Ma range. 1) Yalu River; 2) Siang River; 3) Brahmaputra River; 4) Teesta River; 5) Kameng River; 6) Subansiri River collected south of the Main Frontal Thrust (MFT); 7) Subansiri River collected north of the Main Boundary Thrust (MBT); and 8) Lohit River.

by Cretaceous and Early Tertiary zircon (Fig. 3-1). Over 65% of dated zircons are <200 Ma. A well-defined maximum at 40–60 Ma accounts for 40% of the zircon. Another age cluster accounting for 12% of the zircon occurs between 450 Ma and 650 Ma with a maximum near 530 Ma. Lesser quantities of zircon yield ages in the 700–1200 Ma range with no maxima defined. Roughly 8% of the zircon has $^{207}Pb/^{206}Pb$ ages in excess of 1.2 Ga with no statistically meaningful maxima present.

3.3.1.2. Siang River. Sample SC-03-26-08-6 (location 2 in Fig. 1) was collected near Pashigat, ~550 km down stream from AY06-28-06-1. About 25% of the zircon is <200 Ma (Fig. 3-2). Most is distributed between 40–90 Ma and 110–130 Ma. A high concentration (17%) of older zircon occurs between 450 Ma and 570 Ma while another 20% is between 700–1400 Ma with peaks at 815 Ma, 1.0 Ga, and between 1.1 Ga and 1.3 Ga. The remaining 30% of zircon has ages >1.3 Ga with the only distinct peak at 1.6 Ga.

3.3.1.3. Brahmaputra River. Sample AY02-21-06-2 (location 3 in Fig. 1) was collected near Tezpur, about 900 km downstream from the Yalu River sample and 350 km downstream from the Siang River site. The percentage of <200 Ma zircon is 10% (Fig. 3-3). The <200 Ma zircon is

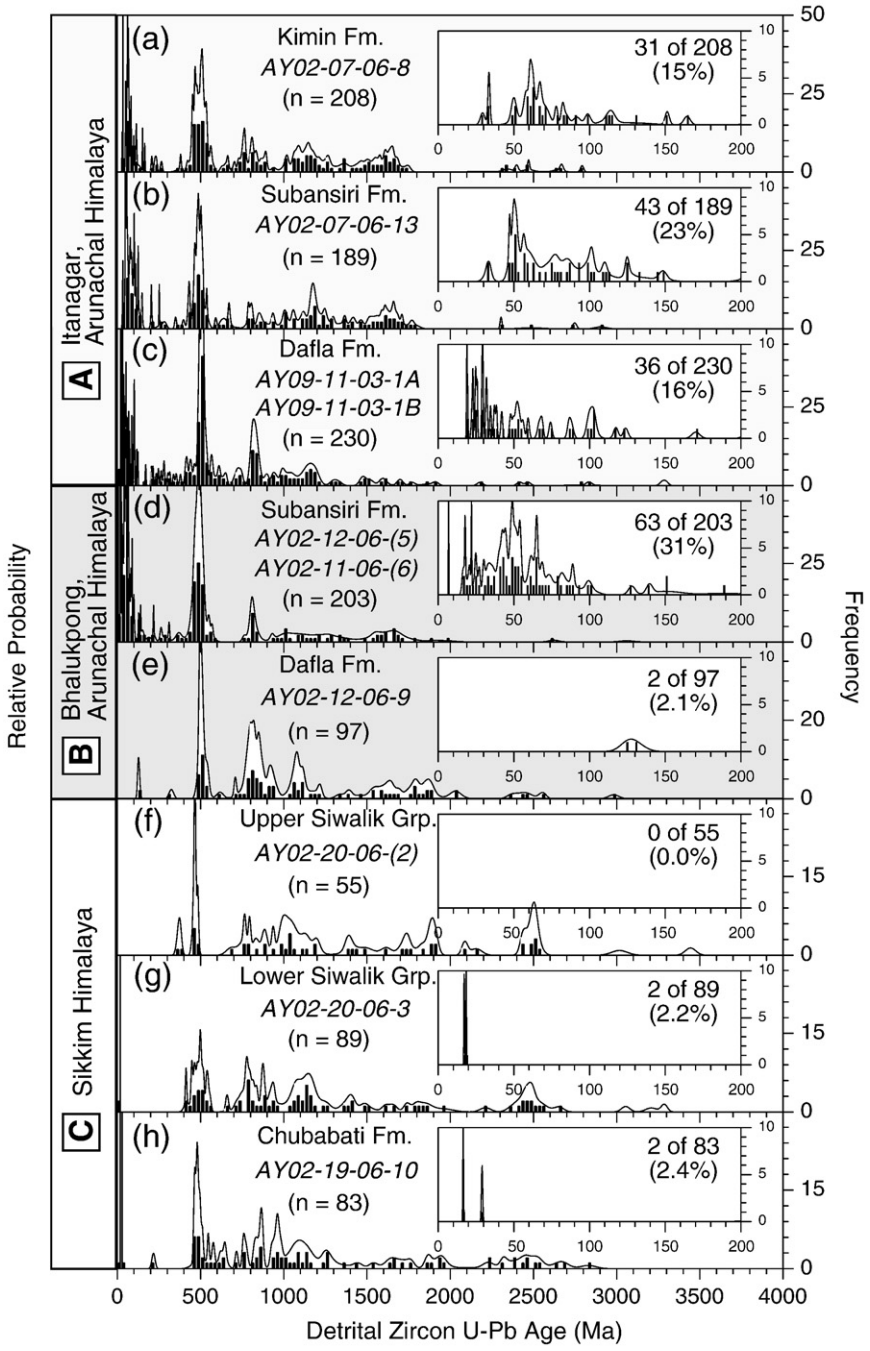

Fig. 4. Histograms and relative probability plots of detrital zircon U–Pb age distributions from Neogene foreland basin deposits labeled A–C on Fig. 1. Insets show detail in the 0–200 Ma range. Panels a–c Itanagar area Kimin Fm., Subansiri Fm. and Dafla Fm. respectively (see Figs. 2 and 3A) Panels d–e Bhalukpong area Subansiri Fm. and Dafla Fm. respectively (see Figs. 2 and 3B). Panels f–h Sikkim Himalaya Chubabati Fm. and lower Swialik Grp. and upper Swialik Grp. respectively (see Figs. 2 and 3C).

broadly distributed between 30 Ma and 130 Ma without distinct age peaks. About 10% of the zircon falls between 450 Ma and 550 Ma with a peak near 500 Ma. Most of the (70%) of the zircon forms a broad distribution between 700 Ma and 1.9 Ga, with weakly defined clusters at 860 Ma, 1.1 Ga, 1.3 Ga, 1.6 Ga, and 1.75 Ga.

3.3.2. Transverse Himalayan Rivers

3.3.2.1. Teesta River. The Teesta River is the westernmost transverse river we sampled. Sample SK08-A was collected within a large sandbar in a floodplain south of the MFT (location 4 in Fig. 1) and contains 3%< 200 Ma zircon. The largest peak in the distribution occurs at 500 Ma, with nearly 50% of all zircon falling between 400–500 Ma (Figs. 3–4). Smaller clusters occur around 900 Ma and between 1.8 and 1.8 Ga, with the latter containing approximately 12% of the zircon sample. The remaining 12% of grains are between 1.9 and 2.8 Ga with no significant peaks.

3.3.2.2. Kameng River. Sample AY02-23-06-1 was collected at the outlet of the Kameng River into the modern foreland basin (location 5 in Fig. 1). The sample lacks ages between 30 Ma and 200 Ma (Figs. 3–5), but contains solitary ages at 25 Ma and 230 Ma. Nearly 40% of the zircon ages fall between 450 Ma and 650 Ma with a peak at 500 Ma. An additional 40% of the zircon is distributed between 750 Ma and 1.2 Ga and clustered at 750–850 Ma and 1.1–1.2 Ga, respectively. While 18% of the zircon is older than 1.2 Ga, no significant age peaks occur.

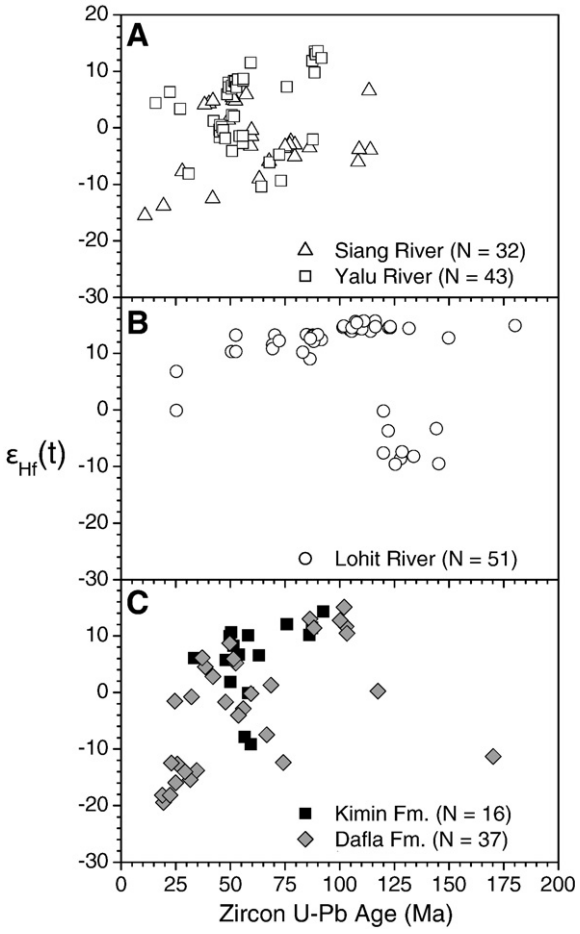

Fig. 5. Lu–Hf results from 0–200 Ma zircons previously analyzed for U–Pb age. Hf isotopic compositions, $\varepsilon_{Hf}(0)$, are calculated values that extrapolate measured present-day $^{176}Hf/^{177}Hf$ ratios back to the time of zircon crystallization. A. Results from modern sands of the Yalu and Siang Rivers. B. Results from Lohti River modern sand. C. Results from Neogene foreland basin strata (Dafla and Kimin Fms.) from the Itanagar area of the Arunachal Himalaya.

3.3.2.3. Subansiri River. Although the Subansiri River is a transverse river like the Kameng, its catchments extend well north of the Himalayan crest (Fig. 1). Sample SC-03-26-08-4 was collected just south of the range front (location 6 in Fig. 1). It contains 18%<200 Ma zircon with the largest concentration between 70–100 Ma (Figs. 3–6). A smaller cluster also occurs at 40–50 Ma. About 30% of the U–Pb ages fall between 450–550 Ma with a strong peak near 500 Ma. Age clusters between 700–900 Ma, and 1.1–1.3 Ga are defined by 18% and 10% of the zircon respectively. Although 17% of the zircon in the sample is older than 1.3 Ga, the only notable concentration occurs between 2.4 to 2.6 Ga.

Due to the possibility that sample SC-03-26-08-4 might contain a significant amount of reworked Tertiary and younger sediment, we collected an additional sample, AY01-05-09-1A, further upstream near the town of Daporijo, north of the Main Boundary Thrust (MBT) (location 7 in Fig. 1). This sample contains only 3 out of 101 grains younger than 200 Ma, aged 22.8 ± 0.2 Ma, 43.0 ± 0.2 Ma and 44.2 ± 1.7 Ma. About 60% of the detrital U–Pb ages are between 450 Ma and 550 Ma, with another 20% between 700 Ma and 900 Ma. There is a very small Middle Proterozoic concentration (<10%) and with the oldest grain in the sample aged 1384.0 ± 69.6 Ma.

3.3.3. Northernmost Indo-Burma Range rivers

3.3.3.1. Lohit River. Sample SC-03-26-08-5 was collected at the intersection of the river with the local topographic front created by active contractional structures (location 8 in Fig. 1). The Lohit River sample yields 36% zircon with ages <200 Ma (Figs. 3–7). Latest Jurassic and Early Cretaceous zircon U–Pb zircon ages are dominant in (100–150 Ma). Early Paleozoic–latest Neoproterozoic zircon is scarce. About 9% of the zircon occurs between 1.0 to 1.25 Ga. The highest concentration (42%) of zircon in the Lohit River is broadly distributed between 1.9–3.0 Ga with no definitive peaks present.

3.4. U–Pb age results from Neogene strata in the Himalayan foreland basin

3.4.1. Itanagar area, Arunachal Himalaya, locality A

We analyzed two samples from the Upper Miocene Dafla Formation (09-11-03-1A and 09-11-03-1B), one from the Upper Miocene Subansiri Formation (AY02-07-06-13), and one from the Pliocene Kimin Formation (AY02-07-06-8). The stratigraphic positions of the samples are shown on Fig. 2. Because the two Dafla samples were collected in close proximity and yield age distributions that are statistically indistinguishable (see discussion in Section 4 on data analysis) we elected to pool the data (Fig. 4a–c). All three formations yield significant concentrations of <200 Ma zircon at 16% (combined Dafla sample), 23% (Subansiri sample), and 15% (Kimin sample). Overall, 18% of the 627 zircons analyzed yield <200 Ma U–Pb ages. The majority of the young zircons are between 40 Ma and 110 Ma with the most prominent clusters at 40–70 Ma. All three units yield high concentrations of 450–550 Ma zircon and Proterozoic zircon with age clusters at 800 Ma, 1.15 Ga, and 1.65 Ga.

3.4.2. Bhalukpong area, Arunachal Himalaya, locality B

We analyzed three samples in the Bhalukpong area, including one from the Upper Miocene Dafla Formation (AY02-12-06-9) and two from the Upper Miocene Subansiri Formation (AY02-12-06-5, AY02-12-06-6; Figs. 1 and 2). We combined the age distributions measured from the two Subansiri samples because they are statistically indistinguishable (see section DR 2 in the Supplementary material). The Bhalukpong area results are shown in Fig. 4d and e. The Dafla sample contains 2% of the total zircon grains with ages <200 Ma at 125 Ma and 130 Ma. Alternatively, 31% of the U–Pb analyses from the pooled Subansiri sample were <200 Ma. Ages yielded by the young zircons define a broad distribution between 20 Ma and 110 Ma with the strongest age cluster between 40 Ma and 60 Ma. Both the Dafla and Subansiri samples exhibit strong peaks at 500 Ma and a broad distribution of Proterozoic ages between 700 Ma and 1.9 Ga with clusters at 800 Ma, 1.15 Ga, and 1.65 Ga.

3.4.3. Sikkim Himalaya, locality C

Three samples of Tertiary sandstone from the Sikkim Himalaya were analyzed (Figs. 1 and 2): one from the upper part of the Lower–Middle Miocene Chunabati Formation (AY02-19-06-10) and two from the Upper Siwalik Group (AY02-20-06-3 and AY02-20-06-2 respectively). The U–Pb age distributions from all the three samples are shown in Fig. 4f,g and h. All samples define a strong peak near 500 Ma and display a broad distribution of Proterozoic and Archean ages with clusters at 700–1200 Ma and 2.4–2.7 Ga. Four of the 227 analyses obtained (1.8%) yield U–Pb ages between 16 and 29 Ma. The provenance signature appears to have evolved with time. The oldest sample from the Chunabati Formation (Fig. 2) contains a 217 Ma zircon and the lowest concentration of 2.4–2.7 Ga zircon (Fig. 4h). The two younger Siwalik samples have higher concentrations of 2.4–2.7 Ga zircon.

3.5. Lu–Hf isotopic results

Previous workers have concluded that the segments of the Jurassic–Early Cenozoic arc in Southern Tibet and the Indo-Burma Ranges have different Hf isotopic compositions (Chu et al., 2006; Liang et al., 2008). Consequently, we have performed detrital zircon Lu–Hf analyses from modern sands of the Yalu, Siang, and Lohit Rivers as well as the Kimin and

Table 2
Kolmogorov–Smirnoff comparison (tertiary strata vs. modern river sands).

	Yalu River	Siang River	Brahmaputra River	Kameng River	Subansiri R. (S of MFT)	Subansiri R. (N of MBT)	Lohit River	Teesta River
Dafla Fm. (Itanagar [A])	7E-32	2E-04	5E-10	4E-04	**0.12**	9E-04	2E-17	0.003
Subansiri Fm. (Itanagar [A])	2E-21	**0.04**	9E-06	3E-05	**0.23**	8E-08	7E-16	0.001
Kimin Fm. (Itanagar [A])	1E-32	**0.04**	1E-04	4E-03	**0.27**	5E-08	1e-15	0.004
Dafla Fm. (Bhalukpong [B])	1E-32	1E-07	**0.02**	**0.06**	3E-06	4E-13	2E-09	4E-07
Subansiri Fm. (Bhalukpong [B])	6E-15	5E-04	9E-15	5E-11	2E-06	1E-05	4E-17	2E-06
U. Siwalik Gr. (Teesta [C])	6E-21	1E-04	**0.02**	3E-05	2E-07	8E-15	2E-05	6e-05
L. Siwalik Gr. (Teesta [C])	9E-30	3E-05	**0.17**	3E-04	3E-06	2E-14	1E-06	9E-06
Chubabati Fm. (Teesta [C])	3E-28	2E-05	**0.17**	1E-03	5E-06	5E-15	3E-06	7E-05

Bold values indicate a high degree of similarity with values >0.05 indicating the distributions are indistinguishable at 95% confidence.

Dafla Formation samples from the Itanagar area (Fig. 1) to test the utility of combined U–Pb and Lu–Hf as a refined provenance tool in this setting (see also Bodet and Scharer, 2000; Wu et al., 2007). Our specific goal was to determine if the Hf isotopic signature of the Gangdese batholith-derived detritus in the river sands varied along strike as implied by the basement Hf results of Chu et al. (2006) and Liang et al. (2008).

Measured present-day ε_{Hf} values of 0–200 Ma zircons were extrapolated to initial values at the time of zircon crystallization using the Lu–Hf decay constants of Söderlund et al. (2004). The resulting array of age-corrected ε_{Hf} values range from primitive (+10 to +15) to highly evolved −10 to −15 (Fig. 5A). Cretaceous zircons yield the most primitive compositions while Oligo–Miocene zircons tend to yield more evolved Hf isotopic ratios,. However, ε_{Hf} values as low as −10 persist over the entire age range. Overall, rivers draining the Gangdese batholith both west (Yalu and Siang Rivers) and east (Lohit River) of the eastern Himalayan syntaxis exhibit no clearly resolvable variation of ε_{Hf} values. When ε_{Hf} and U–Pb age are combined however, distinctly different clusters emerge for the Yalu and Siang Rivers (Fig. 5A) vs. the Lohit River (Fig. 5B).

Detrital zircons sampled from the Dafla and Kimin Formations of the Itanagar area are shown in Fig. 5C. As indicated, the results from the Itanagar Neogene strata more closely resemble the Yalu and Siang field (southern Tibet) than the Lohit River (northernmost Indo-Burma Ranges).

4. Data analysis

4.1. Comparisons between modern sand and Neogene sandstone samples

Quantitative assessment of the similarity of the modern river sands and the Neogene foreland basin deposits requires a general yet simply understood nonparametric method for comparing distributions. The two-sample Kolmogorov–Smirnov (K–S) provides such a measure (Press et al., 1988). In the K–S test, the probability that two distributions are drawn from the same population is given by the parameter *PROB*. This parameter is calculated from the maximum separation (*D*) of two cumulative probability distributions (measured parallel to the cumulative probability axis) and the respective sample sizes. A *PROB* value of 0.05 or higher indicates that the two distributions are indistinguishable at 95% confidence.

Comparisons between the Neogene sandstones and the modern river sands are listed in Table 2. All Neogene strata of the Itanagar area (locality A in Fig. 1) are indistinguishable from the Subansiri River sand collected south of the Main Frontal Thrust at 95% confidence, however all strata are easily distinguished from the Subansiri River sand north of the MBT. The samples of the Kimin and Subansiri Formations are barely distinguished from the Siang River (Both yield *PROB* values of 0.04) due to a lower proportion of 500 Ma zircon and a higher amount of Paleoproterozoic and Archean zircon in the Siang River sample. In the Bhalukpong area (locality B in Fig. 1), the samples from Subansiri Formation are most similar to the Siang River but are readily distinguished from it by a deficit of 500 Ma zircon and an abundance of Paleoproterozoic and Archean zircons in the Siang River sample. Alternatively, the age distribution of the Dafla sample in the Bhalukpong area is indistinguishable from that of the Kameng River sample at 95% confidence (*PROB* = 0.06); it is also relatively similar to the age distribution of the modern sand from the Brahmaputra River sample (*PROB* = 0.02). Farther west in Sikkim (locality C in Fig. 1), age distributions of the Neogene samples most closely match that of the Brahmaputra River sand, with the older two Sikkim samples yielding age distributions indistinguishable from the Brahmaputra River sample at 95% confidence. This close similarity is probably best explained by the fact that both the Brahmaputra river sand and the Sikkim Neogene sandstones are sourced to a great extent from the rocks of the Himalayan orogen.

4.2. Mixing calculations

We performed mixing calculations to systematically assess whether sediment from different regions in Fig. 1 could have blended together to produce the observed age distributions obtained from the Neogene samples in the Arunachal Himalaya. All calculations involve two-component mixing between one proxy representing Himalayan-derived sediment and another representing sediment derived from the Lhasa terrane. We use the age distribution of the Kameng River sample to represent the former and age distributions of the Yalu and Lohit River samples as proxies for the latter. Comparisons of the synthetic age distributions are made relative to a composite age distribution derived from the four samples of the Itanagar area. The *PROB* value for 100% Kameng River when compared with this composite is 0.0003. Kameng–Yalu mixtures with 15–40% of the Yalu River age distribution closely match the age distribution of the Itanagar Neogene samples at 95% confidence (Fig. 6A and B). The best-fit mixture involves 24% of the Yalu River age distribution (*PROB* = 0.44).

An important reason that the incorporation of the Yalu River age components into the Kameng River age distribution so readily matches the Itanagar Neogene samples is that the Paleozoic and the older portion of the age distributions closely resemble each other (Fig. 6B). The same is not true when mixing the Lohit age distributions with the Kameng River ages. The Lohit age distribution differs from that obtained from the Itanagar Neogene samples, particularly with respect to the lack of 500 Ma zircon and the greater abundance of Paleoproterozoic and Archean zircons (Fig. 3-6). The best-fit Lohit–Kameng mixture has 16% Lohit and a *PROB* value of only 0.002 (Fig. 6A and C). The above calculations demonstrate that the age distributions of the Itanagar Neogene samples have the highest affinity with a Gangdese batholith source north of the Himalaya. The same conclusion holds for mixing calculations undertaken with Subansiri Formation samples from the Bhalukpong area, implying that those have a Tibetan source as well.

5. Discussion

5.1. Overview

Our detrital zircon results of Neogene samples have confirmed Cina et al.'s (2007) finding that appreciable concentrations of Cretaceous and Cenozoic zircon attributable to the Gangdese batholith are present

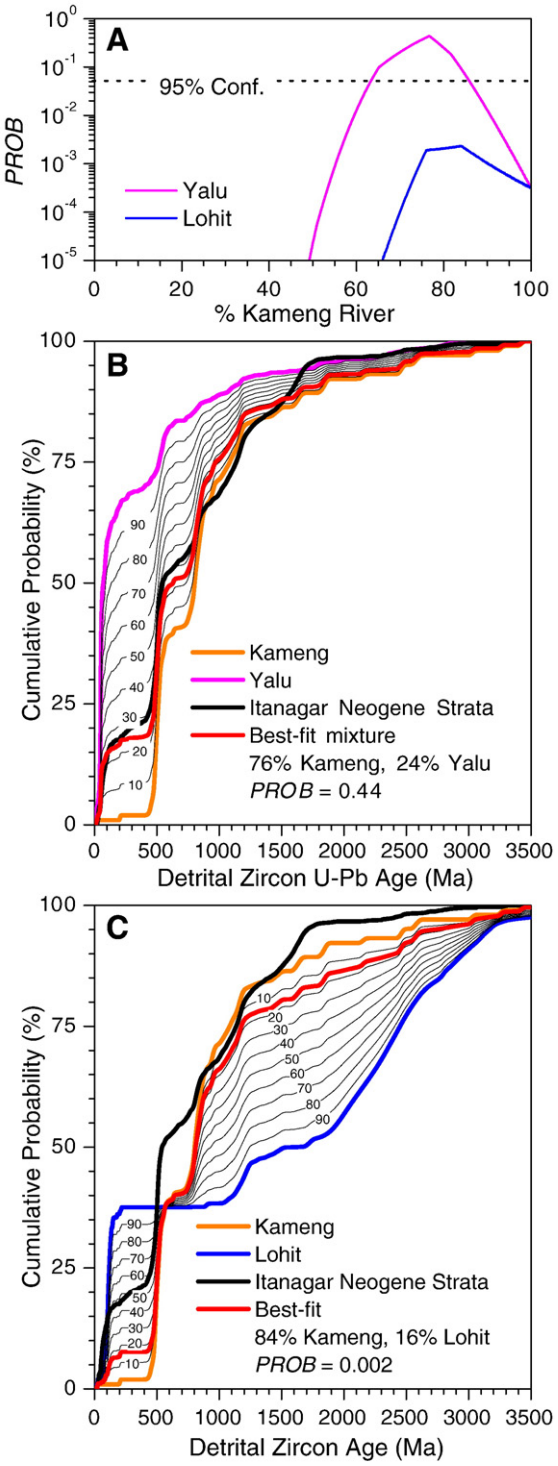

Fig. 6. Binary mixing calculations. Measured detrital zircon U–Pb age distributions from the Yalu and Lohit river sands (proxies for extraregional sediment derived from different segments of Gangdese batholith) are linearly mixed with equivalent data from the Kameng River (proxy for local Himalayan-derived sediment) and compared with a composite age distribution calculated from the Kimin, Subansiri, and Dafla Fms of the Itanagar area. (A) Kolgormorov–Smirnoff (K–S) probability (*PROB*; Press et al., 1988) vs. % Kameng for two mixtures investigated. *PROB* value of 0.05 or higher means river sand mixture produces an age distribution indistinguishable at 95% confidence from Neogene strata. (B)–(C) Cumulative probability plots for mixtures involving Yalu and Lohit Rivers respectively. Only mixtures involving the Yalu River reproduce age distribution of Neogene strata. See text for details.

within the foreland basin of the Arunachal Himalaya (Fig. 4). In detail, Gangdese age zircon is abundant in the Pliocene (Kimin Fm.; Fig. 4a) and Upper Miocene strata (Dafla and Subansiri Fms.; Fig. 4b–c) on both sides of the north-dipping Tipi Thrust in the Itanagar area. In contrast, in the Bhalukpong area, Gangdese-age zircon is present in the Upper Miocene Subansiri strata in the footwall of the Tipi Thrust but absent in the Upper Miocene Dafla Formation in the thrust hanging wall (compare Fig. 4d–e). Finally, the Gangdese-age zircon is completely absent in the Neogene strata of the Sikkim Himalaya (Fig. 4f–g).

Analysis of modern sands of the Yalu–Brahmaputra system documents a significant downstream dilution of Gangdese-age zircon. The Yalu River sand (sample 1 in Fig. 1) consists of 67% Gangdese age zircon (Fig. 3-1), sand from the southern end of the Siang River, ~550 km downstream from the Yalu sample, carries only 26% Gangdese age zircon (Fig. 3-2), and finally, a further ~400 km downstream, the Brahmaputra River only carries ~10% Gangdese-derived zircon. The dilution of the Gangdese zircon along the Siang River can be attributed to the exceedingly high erosion rates across the eastern Himalayan syntaxis (e.g., Garzanti et al., 2004; Stewart et al., 2008), which lies entirely within the Himalayan orogen; whereas dilution of Gangdese zircon in the Brahmaputra River may be caused by further addition of the Himalayan detritus (Fig. 3-3). If the modern relationship between the percentage of Gangdese age zircon and its distance from the source area applies to the past, this implies that Neogene samples containing 15–31% Gangdese-age zircon were most likely deposited by a river that had just flowed past the Himalayan topographic front.

Our sampling of transverse Himalayan Rivers has yielded both expected results and a surprise. The Kameng River drains only the Himalayan orogen, and as anticipated, it produced an age distribution very consistent with the previous studies of detrital zircons from the major eastern Himalayan units (Fig. 3-5; cf. Amidon et al., 2005; Yin et al., 2006; McQuarrie et al., 2008). The Teesta River also has a distinctly Himalayan provenance signature (Fig. 3-4). In contrast, while the Subansiri River sample south of the MFT also exhibits much the same earliest Paleozoic, Neoproterozoic, Mesoproterozoic age clusters as the Kameng and Teesta River samples, it also yields abundant (18%) Cretaceous and Cenozoic Gangdese-age zircon (Fig. 3-6). It is not clear why this Subansiri River sand contains Gangdese age zircon while the Kameng and Teesta River sands do not. The simplest explanation is that the sample we collected consisted primarily of reworked Neogene sediments and was not representative of the modern Subansiri basin north of the MBT. This explanation is strongly supported by the results from the additional sample of modern Subansiri River sand we collected north of the MBT, which contains almost no <200 Ma zircon, and has a detrital U–Pb age distribution similar to those of the Kameng and Teesta Rivers. Outcrops of Cretaceous and younger material are present in the Himalayan orogen, (Zhu et al., 2005b; Aikman et al., 2008), and the small number of <200 Ma grains (3 out of 101 total) in this sample are most likely derived from these younger sources. However, the data suggest that these exposures are not sufficiently widespread in the Subansiri or any other Himalayan catchment to account for the strong abundance of <200 Ma detrital zircon in the Neogene foreland sediments, although more detailed mapping is required to confirm this.

Finally, our sampling of the Lohit River, which drains the eastern Gangdese batholith, revealed important differences in detrital zircon provenance relative to that supplied to rivers farther west, The differences range from subtle (i.e., the lack of an 800 Ma peak) to extreme (i.e., the apparent absence of 500 Ma zircon in the Lohit River catchment (Fig. 3-7). These characteristics allow us to conclude that that the eastern segment of the Gangdese batholith present within the northernmost Indo-Burma Ranges is very unlikely to have supplied the abundant Cretaceous and Cenozoic detrital zircon we observe in the Neogene Arunachal Himalayan foreland basin (Fig. 6), as supported by our mixing calculations in Section 4.2 above.

5.2. Origin of Gangdese batholith zircons in the Himalayan foreland basin

Below, we outline three models for the deposition of Gangdese batholith-derived sediment in the eastern Himalayan foreland basin

(Figs. 7–9). A successful model must: (1) explain how the sediment was delivered to the foreland from the Lhasa terrane west of the eastern syntaxis, (2) account for the high concentrations of Gangdese age zircon, and (3) be consistent with the paleocurrent data in the Neogene foreland basin. Model I involves the simplest possible scenario: The Yalu–Brahmaputra River system has existed in its present configuration since the Late Miocene. Model II invokes a key role for an alternative transverse River (like the modern Subansiri River) as the vehicle by which the Tibetan sediment was routed to the foreland basin. The Subansiri is promising for such a role because its current catchment covers an extensive area north of the Himalayan crest and thus provides a potentially direct pathway between the Lhasa terrane and the Itanagar locality. Deposition of Neogene sediments by the connected Yalu–Subansiri River system can also account for the sedimentologic characteristics of the foreland basin strata that we have studied in the Arunachal area.

Model I, depicted in Fig. 7, holds that the present-day configuration of the Yalu–Brahmaputra River was established by 10 Ma. This view is consistent with those of Burg et al. (1998) who have proposed that the Yalu–Siang–Brahmaputra River system is antecedent to the Himalaya and Brookfield (1998) who alternatively postulated that the Yalu was captured by the Brahmaputra via the Siang River at ca. 10 Ma. As indicated in Fig. 7, Model I positions the Paleo–Brahmaputra River further to the north than it is today to explain how Neogene sediments deposited by the river could have been incorporated into the foreland fold-thrust belt. As Himalayan thrusts propagated forward, the Himalayan topographic front migrated southward, causing the west-flowing Brahmaputra River to shift south to its present-day location.

There are several possible problems with Model I. Firstly, our limited paleocurrent measurements in the Itanagar and Bhalukpong areas suggest deposition from south-flowing rivers, although this can potentially be reconciled with the fact that a large, braided, westward flowing river system would have numerous smaller N–S oriented channels, as does the modern Brahmaputra. Secondly, the percentages of <200 Ma zircon (15–31%) in the Neogene sediments are higher than might be expected after traveling longitudinally across the Himalayan foreland, where there would be a dilution of these zircons by older material derived from the Himalaya as occurs in the modern Brahmaputra River. It is worth noting however, that the significant dilution of Gangdese-derived material occurring at the eastern syntaxis in the modern Brahmaputra River is due in part to the strong coupling between erosion and exhumation of the Namche Barwe massif for at least the last 1 My (Finnegan et al., 2008; Stewart et al., 2008). Prior to the establishment of this feedback, there may have been less of an impact on the concentration of Gangdese detritus as the river traveled across the Himalayan orogen. Lastly, Uddin and Lundberg (1999) have proposed that the Brahmaputra River may have taken a course south of the Shillong Plateau and Mikir Hills during the Miocene, which would preclude the possibility of it depositing sediment at the Itanagar (A) and Bhalukpong (B) localities at that time. If this was the case, an alternate means for delivering Gangdese detritus to the foreland is required.

In Model II (Fig. 8), connection between the Yalu and Brahmaputra Rivers was established at 3–4 Ma, similar to the timing proposed by Zeitler et al. (2001) and Clark et al. (2004). Although sediment eroded from the Gangdese batholith would have been transported toward Indochina prior to 3–4 Ma (see Clark et al., 2004), transient glaciation could have temporarily diverted the Yalu into the Himalayan foreland basin. Montgomery et al. (2004) have identified the remnants of two paleolakes along the Yalu River near the eastern Himalayan syntaxis that were formed by glacial dams within the past 10,000 years. The shoreline of the larger lake stood approximately 680 m above current Yalu River. Zheng (1997) has shown that the advancement of glaciers in the Pamirs dammed large rivers during the Last Glacial Maximum. Neogene topography may have been sufficiently different that a dam of similar scale may have caused the Yalu River to overtop the Himalaya and flow out into the Subansiri River drainage.

The biggest difficulty with Model II is that it cannot explain the persistence of Gangdese batholith provenance within the Neogene

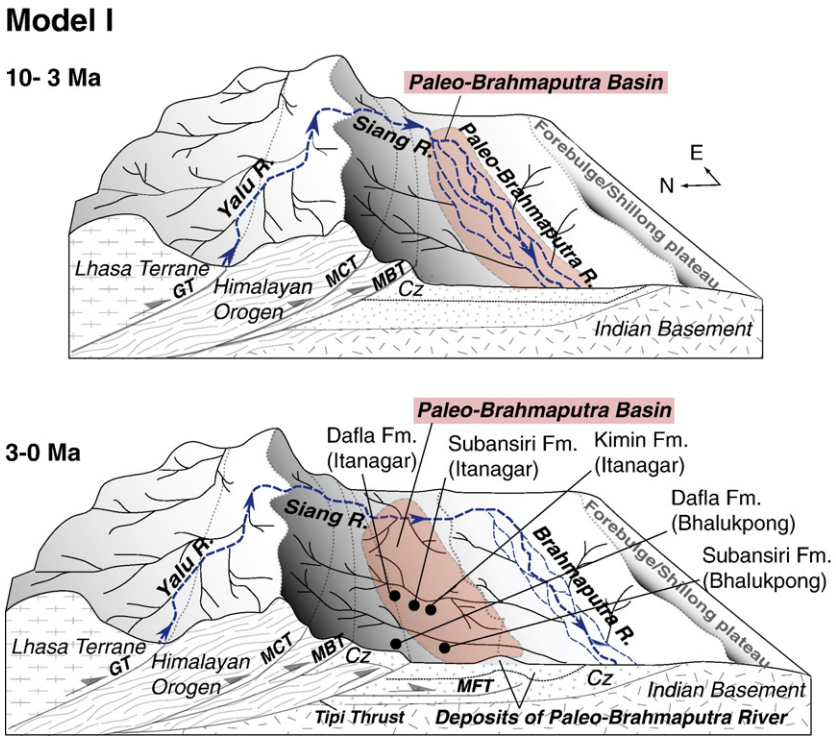

Fig. 7. Model I for the evolution of the Yalu–Brahmaputra River system. Connection between Yalu and Brahmaputra Rivers is established in Late Miocene prior to deposition of Dafla Fm. in Itanagar area of Arunachal Himalaya. Sample positions from Itanagar and Bhalukpong are shown. Southward propagation of Main Frontal Thrust forces Brahmaputra River to migrate southward.

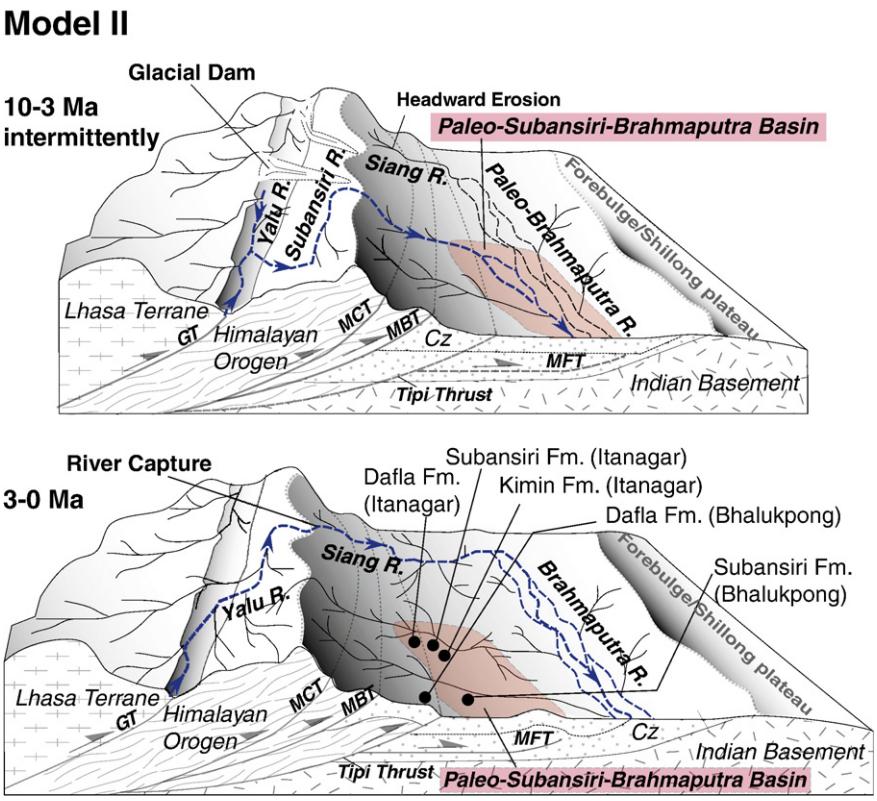

Fig. 8. Model II for the evolution of the Yalu–Brahmaputra River system. Yalu River is intermittently dammed by glaciations and diverted across the Himalayan crest to the foreland basin. Modern Yalu–Brahmaputra River system is established at 3 Ma.

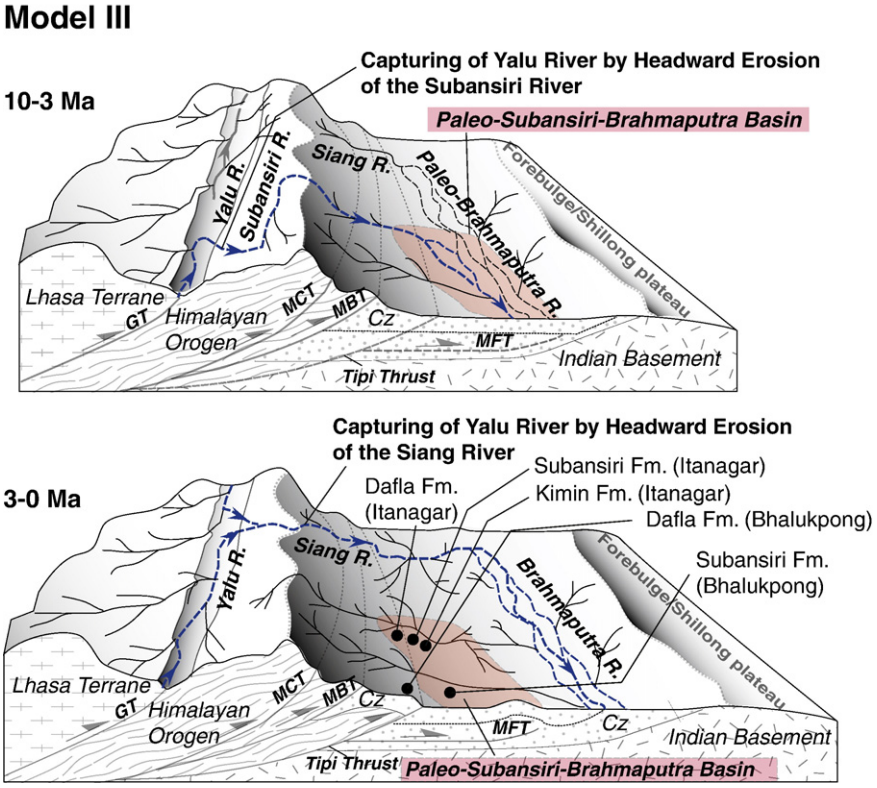

Fig. 9. Model III for the evolution of the Yalu–Brahmaputra River system involving successive capture events by transverse Himalayan Rivers driven by headward erosion. This model invokes capture by the Subansiri River between 10–3 Ma and capture by the Siang River at ~3–4 Ma.

strata of the Itanagar area. This enduring signal can only be explained by deposition by a long-lived river. It is worth noting that glacial dams could also have been present in the scenario presented in Model I. The distinction is that in Model II, a mechanism is required to transport sediment from Lhasa to the foreland prior to ~3–4 Ma, when a direct connection was established via the Siang River.

In Model III, we propose that the Yalu River connected with the Brahmaputra River via a transverse River like the Subansiri from ~10 Ma until the present river course was established via the Siang River at 3–4 Ma (Fig. 9). Burrard and Hayden (1907) first noted that many long feeder streams to the Yalu River flow in the opposite direction to the main Yalu River trunk, suggesting that the Yalu River once flowed westward. Yin (2006) attributed westward to eastward flow reversal of the Ganges River in the Himalayan foreland to diachronous collision and eastward increase in the convergence rate between India and Asia. We speculate that a similar reversal process may have occurred in the Himalayan hinterland for the Yalu River, involving sequential capture events by Himalayan transverse rivers. Model III shows capture of the Yalu River by the Subansiri River during the Late Miocene (Fig. 9). This was followed by capture of the Yalu by the Siang River at 3–4 Ma. Increased headward erosion by the Siang River leading up to this capture event could be related to either the strengthening of the Asian monsoon around this time (Srinivasan and Sinha, 2000) or potentially the initiation of rifting at the Jiacha nickpoint (Fig. 1).

As with Model II, by delivering Gangdese batholith-derived sediment directly across the Himalayan front via the Subansiri River, Model III is consistent with the persistently high concentrations of Gangdese-age zircon in the foreland sediment of the Itanagar area, as well as the observed paleocurrent data, and predicts the presence of Lhasa-derived sediment within the modern Subansiri basin. Model III also makes some testable predictions. For example, the paleo–Yalu–Subansiri River would have deposited Gangdese batholith-derived sediment within the modern Subansiri basin and remnants of these deposits may still be detectable in older river terraces. Additionally, if Model III is true, Upper Miocene foreland sediments east of the Subansiri River should not contain Gangdese-aged detrital zircon. Most significantly, it supports the suggestion of Zeitler et al. (2001) that the coupling between focused erosion and tectonics in the eastern Himalayan syntaxis has only existed at its present strength over the past 3–4 Ma. More data are required to comprehensively evaluate this possibility.

6. Conclusions

We have confirmed the presence of abundant detrital zircon derived from the Gangdese batholith north of the Himalaya within sediment deposited in the eastern Himalayan foreland in two separate localities. This extraregional sediment appears in the Upper Miocene Dafla and Subansiri formations and continues to be present in the Pliocene Kimin Formation. The wealth of the Gangdese-age component in the detrital zircon age distributions of these sediments is comparable to that of modern sand collected at the mouth of the modern Siang River, and suggests that these foreland sediments may have been deposited by a transverse river which had not traveled for a great distance along the Himalayan front. Further sampling and detailed sedimentological study of the foreland sediments is needed in order to determine whether this was the case.

Acknowledgements

This work was made possible by NSF grants to Yin (Tectonics) and Grove (Geochemistry-Petrology), by an ExxonMobil grant to Cina, and by support from DCS-DST and R&D Delhi University for C.S. Dubey and D.P. Shukla. We gratefully acknowledge the analytical support for U–Pb analyses provided by Victor Valencia from the LaserChron Center at the University of Arizona. The LaserChron Center is supported by a grant from NSF's Instrumentation and Facilities Division. George Kamenov and Paul Mueller are thanked for their help with Lu–Hf analyses at the University of Florida. We thank Isabelle Coutard for providing us with the Teesta River sample. Finally, detailed and constructive reviews by Eduardo Garzanti, Djorde Grucic, George Hilley, and an anonymous reviewer greatly improved the content and clarity of the original manuscript.

Appendix A. Supplementary data

Supplementary data associated with this article can be found, in the online version, at doi:10.1016/j.epsl.2009.06.005.

References

Acharyya, S.K., 1999. Tectonic evolution of the Eastern Himalayan Tertiary basin. In: Jain, A.K., Manickavasagam, R.M. (Eds.), Geodynamics of the NW Himalaya, vol. 6. Memoir s of Gondwana Research Group, pp. 263–271.

Acharyya, S.K., 2007. Evolution of the Himalayan Paleogene foreland basin, influence of its litho-packet on the formation of thrust-related domes and windows in the Eastern Himalayas — a review. J. Asian Earth Sci. 31, 1–17.

Acharyya, S.K., Sastry, M.V.A., 1976. Stratigraphy of the Eastern Himalaya. Geological Survey of India, Miscellaneous Publication, New Delhi, pp. 49–65.

Aikman, A.B., Harrison, T.M., Lin, D., 2008. Evidence for Early (>44 Ma) Himalayan crustal thickening, Tethyan Himalaya, southeastern Tibet. Earth Planet. Sci. Lett. 274, 14–23.

Allègre, C.J., et al., 1984. Structure and evolution of the Himalayan–Tibet orogenic belt. Nature 307, 17–22.

Amidon, W.H., Burbank, D.W., Gehrels, G.E., 2005. Construction of detrital mineral populations: insights from mixing of U–Pb zircon ages in Himalayan rivers. Basin Res. 17, 463–485.

Bodet, F., Scharer, U., 2000. Evolution of the SE-Asian continent from U–Pb and Hf isotopes in single grains of zircon and baddeleyite from large rivers. Geochim. Cosmochim. Acta 64, 2067–2091.

Brookfield, M.E., 1998. The evolution of the great river systems of southern Asia during the Cenozoic India–Asia collision: rivers draining southwards. Geomorphology 22, 285–312.

Burg, J.P., Nievergelt, P., Oberli, F., Seward, D., Davy, P., Maurin, J.C., Diao, Z.Z., Meier, M., 1998. The Namche Barwa syntaxis: evidence for exhumation related to compressional crustal folding. J. Asian Earth Sci. 16, 239–252.

Burrard, S.G., Hayden, H.H., 1907. A sketch of the geography and geology of the Himalaya Mountains and Tibet. Superintendent Government printing, Calcutta, India.

Chu, M.F., Chung, S.L., Song, B.A., Liu, D.Y., O'Reilly, S.Y., Pearson, N.J., Ji, J.Q., Wen, D.J., 2006. Zircon U–Pb and Hf isotope constraints on the Mesozoic tectonics and crustal evolution of southern Tibet. Geology 34, 745–748.

Chung, S.L., Chu, M.F., Zhang, Y.Q., Xie, Y.W., Lo, C.H., Lee, T.Y., Lan, C.Y., Li, X.H., Zhang, Q., Wang, Y.Z., 2005. Tibetan tectonic evolution inferred from spatial and temporal variations in post-collisional magmatism. Earth Sci. Rev. 68, 173–196.

Cina, S., Yin, A., Gehrels, G., Grove, M., Dubey, C.S., 2007. Detrital zircon geochronology of Tertiary and modern sediments in the eastern Himalaya: implications for large scale drainage reorganization. Geol. Soc. Am. Abstr. Progr. 39, 593.

Clark, M.K., Schoenbohm, L.M., Royden, L.H., Whipple, K.X., Burchfiel, B.C., Zhang, X., Tang, W., Wang, E., Chen, L., 2004. Surface uplift, tectonics, and erosion of eastern Tibet from large-scale drainage patterns. Tectonics 23, TC1006.

Clift, P.D., Van Long, H., Hinton, R., Ellam, R.M., Hannigan, R., Tan, M.T., Blusztajn, J., Duc, N.A., 2008. Evolving east Asian river systems reconstructed by trace element and Pb and Nd isotope variations in modern and ancient Red River–Song Hong sediments. Geochem. Geophys. Geosys. 9, Q04039.

Coulon, C., Maluski, H., Bollinger, C., Wang, S., 1986. Mesozoic and Cenozoic volcanic rocks from central and southern Tibet: $^{40}Ar/^{39}Ar$ dating, petrological characteristics and geodynamical significance. Earth Planet. Sci. Lett. 79, 281–302.

Debon, F., Le Fort, P., Sheppard, S.M.F., Sonet, J., 1986. The four plutonic belts of the Transhimalaya–Himalaya: a chemical, mineralogical, isotopic, and chronological synthesis along a Tibet–Nepal section. J. Petrol. 21, 219–250.

DeCelles, P.G., Gehrels, G.E., Quade, J., Ojha, T.P., 1998. Eocene–Early Miocene foreland basin development and the history of Himalayan thrusting, western and central Nepal. Tectonics 17, 741–765.

DeCelles, P.G., Gehrels, G.E., Najman, Y., Martin, A.J., Carter, A., Garzanti, E., 2004. Detrital geochronology and geochemistry of Cretaceous–Early Miocene strata of Nepal: implications for timing and diachroneity of initial Himalayan orogenesis. Earth Planet. Sci. Lett. 227, 313–330.

Ding, L., Zhong, D.L., Yin, A., Kapp, P., Harrison, T.M., 2001. Cenozoic structural and metamorphic evolution of the eastern Himalayan syntaxis (Namche Barwa). Earth Planet. Sci. Lett. 192, 423–438.

Ding, L., Kapp, P., Wan, X., 2005. Paleocene–Eocene record of ophiolite obduction and initial India–Asia collision, south central Tibet. Tectonics 24, TC3001. doi:10.1029/2004TC001729.

Dong, G., Mo, X., Zhao, Z., Guo, T., Wang, L., Chen, T., 2005. Geological constraints on magmatic underplating of the Gandese belt in the India–Eurasia collision: evidence of SHRIMP 2 U–Pb dating. Acta Geol. Sin. 79, 801–808.

Finnegan, N.J., Hallet, B., Montgomery, D.R., Zeitler, P.K., Stone, J.O., Anders, A.O., Yuping, L., 2008. Coupling of rock uplift and river incision in the Namche Barwa–Gyala Peri massif, Tibet. Geol. Soc. Amer. Bull. 120, 142–155.
Garzanti, E., Le Fort, P., Sciunnach, D., 1999. First report of Lower Permian basalts in South Tibet: tholeiitic magmatism during break-up and incipient opening of Neotethys. J. Asian Earth Sci. 17, 533–546.
Garzanti, E., Vezzoli, G., Ando, S., France-Lanord, C., Singh, S.K., Foster, G., 2004. Sand petrology and focused erosion in collision orogens: the Brahmaputra case. Earth Planet. Sci. Lett. 220, 157–174.
Gehrels, G.E., DeCelles, P.G., Ojha, T.P., Upreti, B.N., 2006. Geologic and U–Pb geochronologic evidence for Early Paleozoic tectonism in the Dadeldhura thrust sheet, far-west Nepal Himalaya. J. Asian Earth Sci. 28, 385–408.
Guynn, J.H., Kapp, P., Pullen, A., Heizier, M., Gehrels, G., 2006. Tibetan basement rocks near Amdo reveal "missing" Mesozoic tectonism along the Bangong suture, central Tibet. Geology 34, 505–508.
Harris, N.B.W., Xu, R., Lewis, C.L., Hawkesworth, C.J., Zhang, Y., 1988. Isotope geochemistry of the 1985 Tibet geotraverse, Lhasa to Golmud. Philos. Trans. R. Soc. Lond. A 327, 263–285.
Harrison, T.M., Yin, A., Grove, M., Lovera, O.M., Ryerson, F.J., Zhou, X.H., 2000. The Zedong Window: a record of superposed Tertiary convergence in southeastern Tibet. J. Geophys. Res. 105, 19211–19230.
Hayden, M.M., 1907. The geology of the provinces of Tsang and U in central Tibet. Mem. Geol. Soc. India 36 (pt. 2), 122–201.
Heron, A.M., 1922. Geological results of the Mt. Everest reconnaissance expedition. Mem. Geol. Surv. India 54 (pt. 2), 215–234.
Hodges, K.V., 2000. Tectonics of the Himalaya and southern Tibet from two perspectives. Geol. Soc. Amer. Bull. 112, 324–350.
Honegger, K., Dietrich, V., Frank, W., Gansser, A., Thöni, M., Trommsdorff, V., 1982. Magmatism and metamorphism in the Ladakh Himalayas (the Indus-Tsangpo suture zone). Earth Planet. Sci. Lett. 60, 253–292.
Kapp, J.L.D., Harrison, T.M., Kapp, P.A., Grove, M., Lovera, O.M., Lin, D., 2005. The Nyainqentanglha Shan: a window into the tectonic, thermal and geochemical evolution of the Lhasa block, southern Tibet. J. Geophys. Res. 110. doi:10.1029/2004JB003330.
Koons, P.O., Zeitler, P.K., Chamberlain, C.P., Craw, D., Meltzer, A.S., 2002. Mechanical links between erosion and metamorphism in Nanga Parbat, Pakistan Himalaya. Am. J. Sci. 302, 749–773.
Kumar, G., 1997. Geology of Arunachal Pradesh. Geol. Soc. India, Bangalore.
LeFort, P., 1996. Evolution of the Himalaya. In: Yin, A., Harrison, T.M. (Eds.), The Tectonics of Asia. InCambridge University Press, New York, pp. 95–106.
LeFort, P., Raï, S.M., 1999. Pre-Tertiary felsic magmatism of the Nepal Himalaya: recycling of continental crust. J. Asian Earth Sci. 17, 607–628.
Liang, Y.H., Chung, S.L., Liu, D., Xu, Y., Wu, F.Y., Yang, J.H., Wang, Y., Lo, C.H., 2008. Detrital zircon evidence from Burma for reorganization of the eastern Himalayan river system. Am. J. Sci. 308, 618–638.
McQuarrie, N., Robinson, D., Long, S., Tobgay, T., Grujic, D., Gehrels, G., Ducea, M., 2008. Preliminary stratigraphic and structural architecture of Bhutan: implications for the along strike architecture of the Himalayan system. Earth Planet. Sci. Lett. 272, 105–117.
Medlicott, H.B., 1868. The Alps and the Himalaya, a geological comparison. Q. J. Geol. Soc. Lond. 24, 34–52.
Miller, C., Schuster, R., Klotzli, U., Frank, W., Purtscheller, F., 1999. Post-collisional potassic and ultrapotassic magmatism in SW Tibet: geochemical and Sr–Nd–O isotopic constraints for mantle source characteristics and magma genesis. J. Petrol. 40, 1399–1424.
Mo, X., Zhao, Z., Deng, J., Flower, M., Yu, X., Lui, Z., Li, Y., Zhou, S., Dong, G., Zhu, D., Wang, L., 2006. Petrology and geochemistry of postcollisional volcanic rocks from the Tibetan plateau: implications for lithosphere heterogeneity and collision-induced asthenosphere flow. In: Dilek, Y., Pavlides, S. (Eds.), Postcollisional Tectonics and Magmatism in the Mediterranean Region and Asia: Geol. Soc. Am. Spec. Pap., vol. 409.
Mo, X., Hou, Z., Niu, Y., Dong, G., Qu, X., Zhao, Z., Yang, Z., 2007. Mantle contributions to crustal thickening during continental collision: evidence from Cenozoic igneous rocks in southern Tibet. Lithos 96, 225–242.
Montgomery, D.R., Hallet, B., Yuping, L., Finnegan, N., Anders, A., Gillespie, A., Greenberg, H.M., 2004. Evidence for Holocene megafloods down the Tsangpo River gorge, southeastern Tibet. Quat. Res. 62, 201–207.
Mueller, P.A., Kamenov, G.D., Heatherington, A.L., Richards, J., 2008. Crustal evolution in the Southern Appalachian Orogen: evidence from Hf isotopes in detrital zircons. J. Geol. 116, 414–422.
Murphy, M.A., Yin, A., Harrison, T.M., Durr, S.B., Chen, Z., 1997. Significant crustal shortening in south-central Tibet prior to the Indo-Asian collision. Geology 25, 719–722.
Myrow, P.M., Hughes, N.C., Paulsen, T.S., Williams, I.S., Parcha, S.D., Thompson, K.R., Bowering, S.A., Peng, S.C., Ahluwalia, A.D., 2003. Integrated tectonostratigraphic analysis of the Himalaya and implications for its tectonic reconstruction. Earth Planet. Sci. Lett. 212, 433–443.
Najman, Y., 2006. The detrital record of orogenesis: a review of approaches and techniques used in the Himalayan sedimentary basins. Earth Sci. Rev. 74, 1–72.
Najman, Y., Bickle, M., Chapman, H., 2000. Early Himalayan exhumation: isotopic constraints from the Indian foreland basin. Terra Nova 12, 28–34.
Najman, Y., et al., 2008. The Paleogene record of Himalayan erosion: Bengal Basin, Bangladesh. Earth Planet. Sci. Lett. 273, 1–14.
Press, W.H., Flannery, B.P., Teukolsky, S.A., Vetterling, W.T., 1988. Numerical Recipes in C: The Art of Scientific Computing. Cambridge University Press, Cambridge, UK. 994 pp.
Quidelleur, X., Grove, M., Lovera, O.M., Harrison, T.M., Yin, A., Ryerson, F.J., 1997. The thermal evolution and slip history of the Renbu Zedong Thrust, southeastern Tibet. J. Geophys. Res. 102, 2659–2679.
Schärer, U., Xu, R.H., Allègre, C.J., 1984. U–Pb geochronology of the Gangdese (Transhimalaya) plutonism in the Lhasa-Xigaze region, Tibet. Earth Planet. Sci. Lett. 69, 311–320.
Seeber, L., Gornitz, V., 1983. River profiles along the Himalayan arc, as indicators of active tectonics. Tectonophysics 92, 335–367.
Singh, S., Barley, M.E., Brown, S.J., Jain, A.K., Manickavasagam, R.M., 2002. SHRIMP U–Pb in zircon geochronology of the Chor granitoid: evidence for Neoproterozoic magmatism in the Lesser Himalayan granite belt of NW India. Precambrian Res. 118, 285–292.
Söderlund, U., Patchett, P.J., Vertvoot, J.D., Isachsen, C.E., 2004. The ^{176}Lu decay constant determined by Lu–Hf and U–Pb isotope systematics of Precambrian mafic intrusions. Earth Planet. Sci. Lett. 219, 311–324.
Srinivasan, M.S., Sinha, D.K., 2000. Ocean circulation in the tropical Indo-Pacific during early Pliocene (5.6–4.2 Ma): paleobiogeographic and isotopic evidence. Proc. Indian Acad. Sci., Earth Planet. Sci. 109, 315–328.
Stewart, R.J., Halley, B., Zeitler, P.K., Malloy, M.A., Allen, C.M., Trippett, D., 2008. Brahmaputra sediment flux dominated by highly localized rapid erosion from the easternmost Himalaya. Geology 36, 711–714.
Uddin, A., Lundberg, N., 1999. A paleo–Brahmaputra? Subsurface lithofacies analysis of Miocene deltaic sediments in the Himalayan–Bengal system, Bangladesh. Sediment. Geol. 123, 239–254.
Wager, L.R., 1937. The Arun river drainage pattern and the rise of the Himalaya. Geogr. J. 89, 239–250.
Williams, H., Turner, S., Kelley, S., Harris, N., 2001. Age and composition of dikes in Southern Tibet: new constraints on the timing of east–west extension and its relationship to postcollisional volcanism. Geology 29, 339–342.
Wu, F.Y., Clift, P.D., Yang, J.H., 2007. Zircon Hf isotopic constraints on the sources of the Indus Molasse, Ladakh Himalaya, India. Tectonics 26, TC2014. doi:10.1029/2006TC002051.
Xu, R.H., Schärer, U., Allègre, C.J., 1985. Magmatism and metamorphism in the Lhasa block (Tibet): a geochronological study. J. Geol. 93, 41–57.
Yin, A., 2006. Cenozoic tectonic evolution of the Himalayan orogen as constrained by along-strike variation structural geometry, exhumation history, and foreland sedimentation. Earth Sci. Rev. 76, 1–131.
Yin, A., Harrison, T.M., 2000. Geological evolution of the Himalayan–Tibetan Orogen. Annu. Rev. Earth Planet. Sci. 28, 211–280.
Yin, A., Dubey, C.S., Kelty, T.K., Gehrels, G.E., Chou, C.Y., Grove, M., Lovera, O., 2006. Structural evolution of the Arunachal Himalaya and implications for asymmetric development of the Himalayan orogen. Curr. Sci. 90, 195–206.
Zeitler, et al., 2001. Crustal reworking at Nanga Parbat, Pakistan: metamorphic consequences of thermal–mechanical coupling facilitated by erosion. Tectonics 20, 712–728.
Zheng, B., 1997. Glacier variation in the monsoon maritime glacial region since the last glaciation on the Qinghai–Xizang (Tibetan) Plateau. The Changing Face of East Asia During the Tertiary and Quaternary. InCenter of Asian Studies, The University of Hong Kong, pp. 103–112.
Zhu, B., Kidd, W.S.F., Rowley, D.B., Currie, B.S., Shafique, N., 2005a. Age of initiation of the India–Asia collision in the east-central Himalaya. J. Geol. 113, 265–285.
Zhu, D.C., Pan, G.T., Mo, X.X., Wang, L.Q., Liao, Z.L., Jiang, X.S., Geng, Q.R., 2005b. Zircon SHRIMP age of the dacite from the Sangxiu Formation in the Tethyan Himalaya (in Chinese). Chin. Sci. Bull. 50, 375–379.
Zhu, D.C., Pan, G.T., Mo, X.X., Zhao, Z.D., Liao, Z.L., Wang, L.Q., Jiang, X.S., 2006. Geochemistry and petrogenesis of the Triassic volcanic rocks in the east-central segment of Tethyan Himalaya (in Chinese with English Abstract). Acta Petrol. Sin. 22, 804–816.